Characterization of the full complex-valued stiffness tensor of orthotropic viscoelastic plates using 3D guided wavefield data

Adil Han Orta[a,*], Mathias Kersemans[b], Nicolaas Bernardus Roozen[c], Koen Van Den Abeele[a]

[a] *Wave Propagation and Signal Processing (WPSP), Department of Physics, KU Leuven – Campus Kulak, 8500 Kortrijk, Belgium*
[b] *Mechanics of Materials and Structures (MMS), Department of Materials, Textiles and Chemical Engineering, Ghent University, Technologiepark 46, 9052, Belgium*
[c] *Laboratory Acoustics, Division of Soft Matter and Biophysics, Department of Physics and Astronomy, KU Leuven, Celestijnenlaan 200D, B3001 Heverlee, Belgium*

Abstract

A two-stage inversion scheme is proposed to determine the full set of 9 complex-valued stiffness properties of orthotropic viscoelastic plates using their 3D surface velocity response to a broadband vibrational excitation. After converting the surface velocity response to frequency-wavenumber domain by means of a 2D Fast Fourier Transform, the hybrid TLS-ESPRIT and IWC methods are employed to extract complex-valued wavenumber-frequency pairs corresponding to relevant Lamb wave and shear horizontal plate waves from the data. Particle swarm optimization is chosen to inversely determine the orthotropic viscoelastic properties of plate-like objects, using

*Corresponding author. Tel: +3256246024
Email addresses: adilhan.orta@kuleuven.be (Adil Han Orta), mathias.kersemans@ugent.be (Mathias Kersemans), bert.roozen@kuleuven.be (Nicolaas Bernardus Roozen), koen.vandenabeele@kuleuven.be (Koen Van Den Abeele)

the semi-analytical finite element method as a forward model to compute the real and imaginary parts of the wavenumbers. The inversion procedure first identifies the elastic parameters by matching the real wavenumber values, followed by the characterization of the viscoelastic properties which are rather linked to the imaginary wavenumber values. To validate the accuracy of the proposed method, a series of numerical simulations of 3D wavefield data using a finite element model (COMSOL) is conducted, as well as broadband experimental measurements obtained by means of a 3D Infrared Scanning Laser Doppler Vibrometer. The optimization process for each numerical or experimental case study is repeated 20 times to obtain statistics, and the median and median absolute deviation values are reported. It is shown that the inverted orthotropic viscoelastic properties based on the virtual wavefield data are in close agreement with the target values, showing a mean relative error of less than 2% and 5% error on the elastic and viscous properties, respectively. Additionally, the median absolute deviations are negligible showing the robust convergence of the inversion procedure to a global minimum, and giving the confidence to apply the method on experimental wavefield data in order to reveal the full (unknown) C-tensor for material characterization. The proposed characterization method can be used for various orthotropic viscoelastic materials, including metal sheets, carbon/epoxy laminates, and wooden plates.

Keywords: Non-destructive testing, Material characterization, Lamb waves, Viscoelasticity, semi-analytical finite elements (SAFE), Particle swarm optimization, Orthotropy

---

1. Introduction

In the last decades, the development and use of high-performance materials such as fiber-reinforced polymers, or composites in general, has increased rapidly because of their high specific strength and stiffness, exceptional fatigue strength, and good chemical resistance [1]. Additionally, the production flexibility makes it possible to design composites to meet the (structural) requirements for a particular application which is crucial for many engineering components in various demanding industrial sectors such as aeronautics, automobile manufacturing, wind mill blade production, etc. Naturally, the stacking orientation and interaction between fiber and epoxy cause mechanical anisotropy and heterogeneity in composites, leading to a complex elastic wave propagation behavior. As a result, structural health monitoring (SHM) and non-destructive evaluation (NDE) of such composite materials become more advanced compared to isotropic materials such as in homogeneous metals. Yet, for accurate detection, localization and/or assessment of potential damage, the viscoelastic-dynamic behavior of the composite material needs to be thoroughly analyzed [2]. In literature, vibrational and wave propagation methods are generally advertised as the most suitable methods to identify the viscoelastic parameters [3].

In vibrational methods, the material is excited via a shaker or a transducer. Then, the recorded frequency response of the material is used to extract modal parameters, such as natural frequencies, modal damping, modal amplitude, and mode shapes, which can be used to characterize certain material properties [4, 5, 6]. For instance, the extraction of viscoelastic orthotropic material properties for composite laminate beams has been studied by Ko-

rontzis, Vellios, and Kostopoulos [7], leading to the identification of two complex elastic moduli, one complex shear modulus, and one complex poisson ratio by using free vibration of a viscoelastic beam via the Euler–Bernoulli beam theory. Later, transversely isotropic media have been characterized by Melo and Radford based on the reduced parameter nonlinear viscoelastic model and dynamic mechanical analysis (DMA) [8]. An accurate shell element model derived from the higher-order shear deformation theory was used by Matter et al. to extract six elastic parameters and six loss factors [9]. Elasticity and damping properties in sandwich structures with a relatively stiff core were examined by Schwaar et al. [10], providing a characterization of five elastic parameters and five loss factors. A sensitivity study for the elasticity characterization of wood has been conducted by Longo et al. using resonant ultrasound spectroscopy (RUS) [11]. The results revealed that viscoelastic damping might cause overlapping and/or disappearing resonant peaks, which makes it necessary to proceed to the use of mode shapes. Even then, only five or six elastic parameters out of nine could be identified based on the first nine natural frequencies. The problem can be solved by increasing the number of used natural frequencies, but this implies examining a broader frequency regime which can become problematic. Indeed, the identification of viscoelastic parameters for orthotropic plates in the higher frequency range is quite sophisticated due to the requirement for advanced mathematical models and the increasing complexity and importance in realizing appropriate boundary conditions which might lead to large errors in the characterized stiffness parameters.

In wave propagation methods, ultrasonic waves are typically generated

and recorded by using a pair of emitting and receiving transducers. The recorded wave propagation signal characteristics depend on several factors such as the stiffness properties of the material (both the elastic and viscous parts), the geometry of the part, as well as the amplitude and frequency content of the excited signal. Several analytical and numerical methods have been developed to predict the wave propagation behavior and to characterize the (visco)elastic properties. One of the most commonly used methods is based on bulk wave propagation, as proposed in some of the earliest studies in the field by Hosten et al. [12]. This pioneering method has been validated for various plate materials including wood and fiber-reinforced polymers [13, 14, 15]. Although the bulk wave-based characterization method is computationally efficient, it has certain limitations. First of all, as this approach assumes that the medium is infinite in every direction, the ultrasound wavelength has to be much smaller than the plate thickness ($\lambda << d$), which puts a lower boundary on the frequency range. On the other hand, frequency dependent damping characteristics and restrictions on the validity of the homogenization condition put an upper boundary for the "frequency $\times$ thickness" (fd) regime [16, 17]. Secondly, in realistic finite thickness plates, discontinuous phase shifts might occur in the transmitted signals which is in contrast to the infinite body assumption. These phase shifts need to be accounted for in order to invert the stiffness constants with high accuracy [16, 17]. Thirdly, bulk wave methods often require the sample to be immersed in a coupling fluid (generally water), introducing problematic measuring conditions for moisture-sensitive materials, such as wood. And finally, the main axes of orthotropy of the sample under consideration need to be known a

priori in order to correctly identify the material parameters [16, 17].

Lamb wave propagation-based characterization methods can overcome many of the limitations of the bulk wave-based characterization methods. The downside, however, is that Lamb wave-based inversion methods require a more sophisticated forward calculation model, and the typical computational efficiency of such models is lower compared to bulk wave calculation methods. In literature, the elastic properties of orthotropic plates have already been successfully identified in several studies [18, 19, 20, 21]. Additionally, some of the studies are focused on the uncertainty of the extracted stiffness parameters by using a fuzzy-based inversion approach or Bayesian inference scheme with surrogate modeling from experimental guided wave data [22, 23]. However, the next step, which is the characterization of the viscoelastic parameters of orthotropic plates, is more demanding as eighteen parameters (nine elastic and nine viscous) need to be identified. Marchetti et al., for instance, used Hankel functions, equivalent single layer thin plate model and the inhomogeneous wave correlation (IWC) method to identify five flexural rigidities and the corresponding loss factors for composite plates [24, 25]. Even though this method successfully inverted the properties for a transversely isotropic material, it is not capable to identify all eighteen parameters of an orthotropic material because the sensitivity of the out-of-plane (C_{13},C_{23} and C_{33}) stiffnesses is extremely small in the low fd regime, which is consistent with the conclusions reported by Longo et al. for wooden samples [11]. To overcome this problem, an extension of the study to a higher fd regime is necessary, but entails the disadvantage that the negative effect of noise and environmental fluctuations becomes larger in such high-frequency

regimes.

In terms of excitation and recording, the earliest studies, e.g. as conducted by Hosten, used two ultrasonic immersion transducers to excite and measure bulk and Lamb waves in the MHz range in view of identifying the stiffness parameters of an orthotropic plate [26]. As an alternative, and certainly interesting for materials that cannot be examined in immersion conditions, contact transducers can be used, as in the work of Fathi, Kazemirad, and Nasir who studied the moisture-dependent isotropic viscoelastic properties of wood by using two ultrasonic contact transducers operating at a 200 kHz center frequency [27]. Even though the validity of these methods is proven, the use of immersed, contact or even air-coupled transducers in recording mode has certain limitations. Firstly, these methods commonly measure the response along just a single line, which only gives the stiffness for that particular orientation, whereas most of the engineering applications require general 3D stiffness parameters for design and modeling. Secondly, ultrasonic transducers should be coupled with an intermediate medium such as water or air, or attached to the sample. Using water as a coupling medium is impractical for many applications involving porous materials such as wood or isolation foams. On the other hand, air-coupled experiments in the ultrasonic regime exhibit poor efficiency due to the typically large acoustic impedance between air and the analyzed material [28]. Finally, the use of glued or gel-coupled transducers becomes unworkable to efficiently obtain line or surface scans.

In recent years, the recording of wave propagation by ultrasonic transducers is gradually substituted by scanning laser Doppler vibrometry, which

offers a contactless interferometric measurement of the broadband vibration velocity of object surfaces. However, for an optimal acquisition, surface preparation, such as applying retro-reflective tape or small glass bead spray, is generally required to increase the back-scattered laser signal and to improve the signal quality. Recently, scanning laser Doppler vibrometers with infrared lasers and three scanning heads have entered the market [29]. The infrared laser wavelength shows improved sensitivity for a range of technical materials, and yields acceptable signal quality over a wide vibrational frequency range, even for untreated surfaces and obliquely incident laser beam. Furthermore, the angled configuration of the three laser heads allow to extract the three velocity components (both in-plane and out-of-plane velocities) over the measurement surface. In recent studies, the Polytec 3D SLDV-PSV500 XTRA has been intensively used to record Lamb wave propagation wavefield data in 3D for the inversion of the elastic parameters of orthotropic materials [30, 31]. The all-new patented QTec®technology from Polytec will even further enhance the sensitivity. This technology uses a heterodyne multi-path interferometer concept, supported by a parallel signal processing step for four detectors within each of the sensor heads, which considerably avoids speckle dropouts.

To further analyse the acquired data and extract the dispersion and attenuation information, a post-processing procedure is required. As usual in this research field, the recorded (raw) signals at the surface $S(x, y, t)$ consist of a combination of several Lamb wave modes, measurement noise, as well as forward and backward propagating waves due to edge reflections. Various methods have been introduced to extract the complex wavenum-

bers from these pre-processed signals, such as the Fast Fourier Transform (FFT) [32], the time–frequency analysis (TFA) [33], the zero-crossing technique (ZC) [34], the matrix pencil decomposition method (MPDM) [35], the sparse wavenumber analysis (SWA) [36], the spatial Laplace transform (SLT) [37], the inhomogeneous wave correlation (IWC) [38], and the Estimation of Signal Parameters via Rotation Invariant Technique (ESPRIT) [39]. Among these, MPDM, IWC and ESPRIT have already been used and validated for the characterization of material properties [40, 24, 39].

In the present study, a new material characterization method is proposed to identify the homogenized viscoelastic parameters of materials from 3D Lamb wavefield data. The aspiration behind the proposed method is to identify the full set of viscoelastic parameters of arbitrary orthotropic materials by using full field data acquired in the mid fd regime (up to 1.5 MHz.mm) to overcome the limitations of the existing methods. This study is a follow-up of our previous study [41] which focused on the identification of stiffness parameters for elastic materials by using full field Lamb wave data. The novelty of the proposed method is its ability to extract complex wavenumbers via hybrid TLS-ESPRIT (total least square estimation of signal parameters via rotation invariant technique) and the IWC method (inhomogeneous wave correlation method). The extracted complex wavenumbers are essential to identify viscoelastic orthotropic stiffness parameters. To test the accuracy of the proposed method, a series of numerical simulations applying a finite element model (COMSOL) for different materials is studied at first. For the inversion, the semi-analytical finite element (SAFE) method is embedded as a forward model in the two-stage particle swarm optimization (PSO) proce-

dure. The inversion procedure is repeated 20 times to avoid local minima and to obtain statistics on the results. Following the numerical validation, actual Lamb wavefield data measured on carbon epoxy (C/E) and glass fiber (G/F) woven plates is used for the experimental validation. The obtained viscoelasticity results appear highly reasonable and substantiate that the proposed inversion technique can indeed be used to identify the homogenized complex valued stiffness properties of orthotropic viscoelastic plates.

The paper is structured as follows. In Section 2, the most important aspects of the forward model (SAFE) and the optimization procedure (PSO) are recalled. In Section 3, the virtual and actual measurement protocols for COMSOL and for the experimental wavefield acquisition, respectively, are outlined, along with some details about the hybrid ESPRIT-IWC method. In Section 4, the results of the numerical studies as well as of the experiments are presented for different materials.

2. Optimization Procedure

2.1. Forward model SAFE

To efficiently model Lamb wave propagation behavior for use in the optimization procedure, the approximate method called semi analytical finite element method (SAFE) is adopted in this study [42]. The forward model is implemented in a standalone MATLAB toolbox called 'The Dispersion Box', and can be downloaded freely from GitHub [43]. The accuracy as well as the computational efficiency of the method are shown in literature [44]. The method assumes an infinite geometry along the in-plane directions and thus

ignores the effect of reflections coming from edges. Further, it uses a far-field wave propagation equation, neglecting near-field features introduced by the vibrational actuator. In the SAFE method, the medium is discretized in the through-thickness direction, and the stiffness and mass matrices of each element is calculated. By imposing energy equilibrium, the problem transforms into a generalized eigenvalue problem, which is numerically stable [42].

$$[K_1 + ikK_2 + k^2K_3 - \omega^2 M]_M U = 0 \tag{1}$$

The solution of the generalized eigenvalue problem in Eq. 1 supplies the (homogenized) complex wavenumber values, $k = k_r + jk_i$, which are characteristic for the plate material and geometry (thickness and stacking). More precisely, the dispersive variation of the real wavenumber (k_r) values with respect to *fd* provides the dispersion curves which fundamentally relate to the elastic part of the stiffness tensor. On the other hand, the imaginary wavenumber (k_i) values link to the attenuation behavior of the material, and thus essentially to the viscoelastic part of the tensor.

2.2. Inversion Optimizer PSO

For the inverse characterization of material parameters, a proper selection of the optimization algorithm is crucial. Obviously, it should be able to handle the dimensionality, the topology and the size of the parameter search space, and to provide accurate results in a computationally efficient manner [3]. To characterize a homogenized viscoelastic orthotropic plate, a total of eighteen independent parameters (nine elastic and nine viscoelastic) need to be identified. Therefore, it is no longer convenient to use gradient-based

optimization methods, which have a high possibility of converging to a local suboptimal minimum. Heuristic algorithms can overcome the drawbacks of gradient-based algorithms as they achieve stable inversion for even very high dimensional optimization problems. In literature, different optimization algorithms have been proposed for material characterization such as genetic algorithm (GA) [21], particle swarm optimization (PSO) [17, 39], simulated annealing optimization (SAO) [45], and surrogate optimization (SO) [46]. In the present study, PSO was selected and used because of its computational efficiency and superior accuracy, as obtained as the outcome of an extensive study by the authors [46].

The study of bird flock preying behavior serves as the inspiration for the particle swarm optimization (PSO) [47]. Considering that the algorithm uses a heuristic approach and swarm dynamics, the objective function does not need to be differentiable. Briefly recapitulated, the swarm dynamics such as position, speed, and fitness value of each individual particle are first calculated. The position of each particle is then used to determine the best position of the swarm, and this best position is subsequently used as a guide until reaching the global minimum. For the practical implementation of the optimization algorithm, the MATLAB Global Optimization Toolbox™ is used due to its speed, efficiency and accuracy. To improve the convergence and accuracy, the constrained nonlinear multivariable function 'fmincon' is combined with PSO.

After embedding SAFE as the forward model in the hybrid PS-fmincon optimization, it is possible to determine the orthotropic viscoelastic tensor coefficients. To increase the convergence of the algorithm, we propose a

two-stage inversion algorithm in which real and imaginary wavenumbers are employed successively to obtain our premise.

In Stage I, the inversion procedure focuses on the identification of 9 elastic parameters. The procedure is initiated by randomly selected swarm parameters and elastic parameters within the search domain, which is defined by estimates from literature with -40 to $+60\%$ bounds. The non-symmetric boundary conditions are adopted because black-box optimization algorithms tend to take middle points as an initial solution which conflicts the blind search of the parameters. The error between the measured and computed (via SAFE) real wavenumbers is then minimized by updating the elastic parameters (C'), while the viscous parameters (C'') are assumed to be zero during Stage I. The objective function of Stage I is therefore simply defined as the sum of absolute percentage error between the experimental and simulated real wavenumbers:

$$f_{obj_1} = \sum_{i=1}^{F} \sum_{j=1}^{K} \sum_{l=1}^{L} \left| \frac{k_{r,exp}^{i,j,l} - k_{r,sim}^{i,j,l}}{k_{r,exp}^{i,j,l}} \right| \tag{2}$$

where F is the total number of frequencies used, K is the total number of wave modes, and L is the total number of in-plane propagation directions (ϕ). Upon convergence, Stage I yields the best estimation of the nine homogenized elastic parameters of an orthotropic material.

Stage II focuses on matching the imaginary wavenumber values to infer the unknown viscous parameters (C''). Considering that the weak coupling between viscosity and elasticity was ignored in Stage I (the viscous parameters (C'') were set to zero in Stage I), only a small tolerance on the elastic parameters (C') is allowed in Stage II. In particular, the elastic parameters in Stage II are initialized by the optimized values obtained in Stage I, while

the spread is limited to their median absolute deviation (± MAD). The viscous counterparts (C'') are initially set at estimates found in literature with -40 to $+60\%$ bounds. In a case where the viscous stiffness parameters are unknown, certain percentage (between 1% and 5%) of the inverted elastic stiffness parameters are taken as initial guess for the actual viscous stiffness parameters. When the optimization process converges to the pre-set boundaries, the inversion is restarted with new estimates for the corresponding viscosity to prevent the algorithm from converging to the wrong stiffness parameters during the determination of the unknown viscous parameters. As a result, Stage II operates in an 18 dimensional search space, of which 9 dimensions are largely reduced. The congregated objective function of Stage II is specified as:

$$f_{obj_2} = f_{obj_1} + w \sum_{i=1}^{F} \sum_{j=1}^{K} \sum_{l=1}^{L} \left| \frac{k_{i,exp}^{i,j,l} - k_{i,sim}^{i,j,l}}{k_{i,exp}^{i,j,l}} \right| \tag{3}$$

where w is a weighting factor, representing the relative attention of the inversion to the viscosity parameters. In case w is taken too small, large errors might emerge in the viscous tensor. On the other hand, if w is too large, less consideration is given to the inversion of the elastic parameters. Besides, w also allows to take into account the scale difference between real and imaginary wavenumbers. As in this two step approach the elastic parameters as outcome of Stage I are assumed to be close to their optimal values, a value of w equal to 10 is selected in this study.

The flowchart of the complete two stage inversion procedure can be found in Fig. 1. Both stages are repeated 20 times, and median values are reported as the optimized stiffness parameters. Moreover, to evaluate the precision and

robustness of the inversion method, the median absolute deviation MAD for each stiffness parameter is also reported. In all inversion examples considered here, the following input variables for the hybrid optimization variables and search space bounds were assumed:

- Stage I search bounds:
  - $C' \rightarrow$ [-40%;+60%] of the literature values
- Stage II search bounds:
  - $C' \rightarrow C'_{Stage_I} \pm$ MAD
  - $C'' \rightarrow$ [-40%;+60%] of the literature values
- Maximum Iterations: 100
- Swarm Size: 100
- Maximum Stall Iterations: 20
- Interior-point Algorithm (fmincon)
- Maximum Iterations (fmincon): 1000

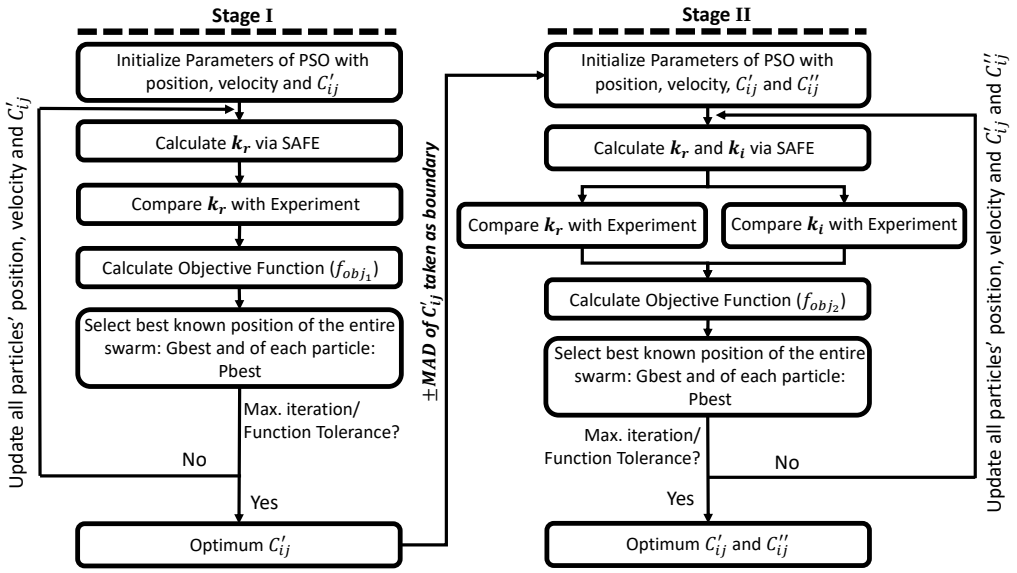

Figure 1: Flowchart of the inversion procedure to determine the viscoelastic stiffness parameters. This entire procedure is repeated 20 times in each case study and for each stage to obtain median values and median absolute deviations on the output parameters.

3. Data generation and conditioning

3.1. Simulation data - COMSOL

To test the accuracy, validity and robustness of the inversion procedure, a finite element model is constructed in COMSOL to numerically compute the wave propagation dynamics for a range of plates for which the actual orthotropic viscoelastic tensor is known. Several aspects of typical 3D finite element models make the computation of the wave propagation behavior over an extended frequency range a quite challenging task. Firstly, as reported in literature, the number of elements per wavelength should ideally be some-

where between 10 and 20 for damped wave propagation [48]. Secondly, to avoid near source transient effects and to observe stabilized wave dynamics, the in-plane size of the plate needs to be large enough. Consequently, millions of degrees of freedom need to be solved in each step, which requires high computational power and time. Alternatively, the model could be simplified by using several 2D finite element mockups, but these models can only be used in principal directions in an orthotropic medium because of the presence of shearing effects in the non-principal propagation directions. For these reasons, a comprehensive 2D semi-analytical finite element model which accounts for the contribution of shearing effects along non-principal wave propagation directions is employed in this study. This 2D SAFE model is computationally efficient and can easily be implemented in COMSOL Multiphysics' Partial Differential Equation Solver following the work of Predoi et al. [49]. Note that the 2D SAFE method from Predoi et al. is fundamentally different from the SAFE method by Bartoli et al. that was introduced earlier, as the former calculates the full wavefield whereas the latter only provides the individual wavenumber-frequency pairs that correspond to potential Lamb & SH waves. The details of the COMSOL simulation model can be found in literature [41] .

3.2. Experimental data – 3D IR SLDV

To experimentally demonstrate the performance of the proposed method, actual wavefield measurements are performed on a $330 \times 330 \times 2$ mm^3 Carbon Epoxy (C/E) UD laminate with stacking sequence $[45/0/-45/90]_s$ and a $600 \times 600 \times 6$ mm^3 glass fiber (G/F) woven laminate with stacking sequence $[45/-45/0/90]_{3s}$. For the excitation, a single piezoelectric actuator (type

EPZ-20MS64W) is positioned at the center of each plate, and is driven by a 100 V_{pp} voltage supplied by a Falco systems WMA-300 voltage amplifier. A broadband sweep sine voltage signal with frequencies between 5 kHz to 300 kHz is used, having a time duration of 16 ms. The full-field 3D vibrational surface response is recorded, on a similar star-like grid as for the above mentioned virtual experiments, by an infrared 3D SLDV (Polytec PSV-500-3D-Xtra) [41]. The three laser heads are set up in an angled configuration in order to measure both the out-of-plane and in-plane vibrational response with good sensitivity. The vibrational response signals are recorded at a sampling rate of 625 kS/s. The C/E layered and G/F woven composite plates are scanned with a grid step $D_r \approx 1$ mm and $D_r \approx 1.25$ mm, respectively. Each scan point is measured 20 times to improve the signal-to-noise ratio. To further improve the measurement quality, the entire surfaces of the plates have been covered with retro-reflective tape. Especially for the recording of the in-plane velocity components, this surface preparation provided a huge improvement in the signal-to-noise ratio, which is crucial for correct identification of imaginary wavenumbers. An example of the recorded time signal is also provided in Fig. 2(a). The total execution time of the experimental scans amounted to around 1 hour. Fig. 2(b) and Fig. 2(c) illustrate a snapshot at a randomly chosen time instance of the recorded vibrational response of the plates in such a star-like configuration corresponding to a discrete set of angles (ϕ between 0 and 180 degrees, $\Delta\phi$=15 degrees).

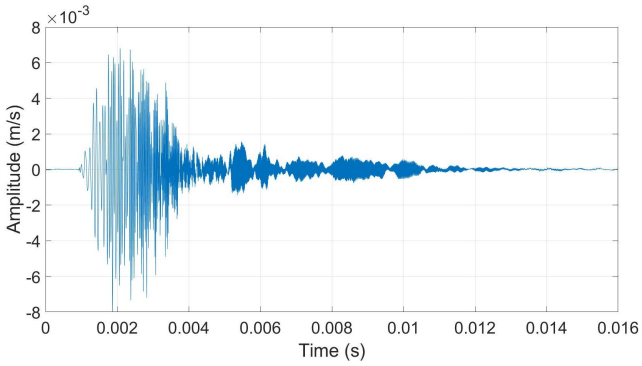

(a)

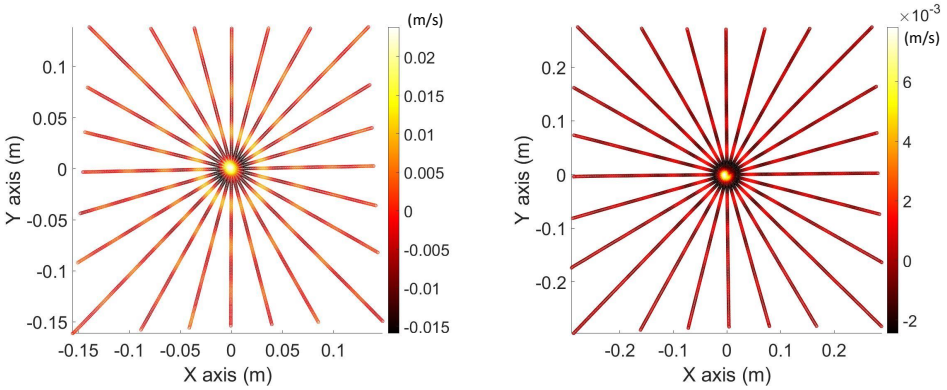

(b) (c)

Figure 2: Wave propagation using a 3D infrared SLDV, a) The out-of-plane response to a broadband sweep excitation (50-300 kHz in 16 ms) recorded on a 5 mm thick UD C/E plate when ϕ=45 at a distance of 15 cm from the actuator, b) The recorded wave propagation on a C/E layered plate at t =1.2 ms along a discrete set of angles, and c) The recorded wave propagation on a G/F woven plate at t =1.2 ms along a discrete set of angles.

3.3. Hybrid ESPRIT-IWC method

As explained before, the proposed two-stage inversion algorithm operates on complex wavenumber-frequency data. To achieve comparable datasets, additional post processing procedures are needed to extract the complex wavenumbers from the experimental and numerical full-field velocity data. For an accurate extraction of the imaginary wavenumbers of the Lamb wave modes, several factors that affect the recorded signals should be considered.

Firstly, the SAFE model uses a far-field wave propagation equation, neglecting near-field features introduced by the vibrational actuator. In literature, it is indicated that the near-field typically end, and far-field effects start after a distance of about a wavelength or three times the largest dimension of the source [35]. Moreover, it is commonly recognized that a better approximation of the attenuation effect of Lamb waves can be obtained for sampling points that are located away from the excitation source. Therefore, only those measurement points that are at least 5 cm away from the piezo-electric actuator were selected and used to overcome near-source effects.

Secondly, the effect of the geometric attenuation for circular waves ($\sqrt{S(r,t)}$ with S the signal and r the propagation distance) needs to be accounted for in order to only retain material damping effects. This can be easily done by correcting the amplitude of the propagating wave signals following the work of Ramadas [50].

Thirdly, wave reflections coming from free edges need to be removed because they interfere with the direct wave signals, leading to changes in the local amplitude. For this reason, the simulated and/or experimentally measured wavefield data along each direction, $S(x, y, t)$ or $S(r\cos(\phi), r\sin(\phi), t)$

or $\tilde{S}^*(r, \phi, t)$ with r the distance to the actuator, and ϕ the in-plane orientation angle, is converted into the frequency-wavenumber domain by means of a 2D Fourier transform yielding $\tilde{S}^*(k, \phi, f)$, and the quadrants of frequency-wavenumber domain that contain backward propagating waves are forced to zero. Then, by taking the inverse Fourier transform, the backward propagating waves are effectively removed, and the amplitude of the signals is corrected. Note however, that for very lightly damped plates, double edge reflections may still appear in the wavefield data as these are not filtered out by the above approach. In such cases, a suitable time windowing could be applied in addition.

Fourthly, the response to the broadband chirp signal used in the experiment to measure the dispersive behavior is recorded in the time-domain, but the final goal is to arrive at the complex wavenumber values which change as function of frequency. To extract the wavenumbers on specific frequencies, the broadband chirp signals are converted into 5 cycle Gaussian windowed tone burst signals following the method of Michaels et al. [51]. To minimize the effect of noise on the recorded data, a rational transfer function is used.

Finally, an appropriate complex wavenumber extraction method needs to be selected and implemented. The matrix pencil decomposition method (MPDM), the estimation of signal parameters via rotation invariant technique (ESPRIT), and the inhomogeneous wave correlation (IWC) method stand out among the variety of complex wavenumber extraction methods because of their established superiority. Whereas MPDM and ESPRIT respectively employ singular value decomposition and eigen-decomposition of the multi-channel covariance matrix, IWC simply optimizes the measured

and simulated wave propagations by changing the wavenumber values. Although IWC shows high accuracy in extracting complex wavenumbers, its disadvantages are that it employs a peak searching algorithm which requires the setting of a threshold and that is not capable of determining the number of modes. Especially for cases where higher-order Lamb modes are available, the determination of the complex wavenumbers becomes more sophisticated, and the IWC algorithm becomes computationally inefficient, in contrast to the MPDM or ESPRIT methods which tend to be more convenient for such cases. As the total least square ESPRIT (TLS-ESPRIT) is found to give much better results compared to the direct MPDM when the noise level is above a certain threshold [52],the TLS-ESPRIT algorithm is adopted in the present study to extract the real wavenumbers and the number of Lamb wave modes. With this knowledge, the IWC approach is employed to subsequently find the imaginary wavenumbers. This hybrid approach thus takes the best of both methods, resulting in a robust extraction of complex wavenumbers from multi-modal data.

The flowchart showing the various phases in the proposed hybrid wavenumber extraction method is outlined in Fig. 3. The blocks that apply to the various steps in the post-processing are indicated in color: Red for the correction due to spreading, Green for the elimination of the back-propagating waves, Blue for Michaels method for the variation in frequency, and Purple for the hybrid TLS-ESPRIT and IWC.

More details on the mathematical formulations of TLS-ESPRIT and IWC can be found in literature [38, 53]. As a final outcome of this algorithm, the extracted complex wavenumber values are individualized, stored and ready

for use in the inversion algorithm for identifying the full viscoelastic tensor.

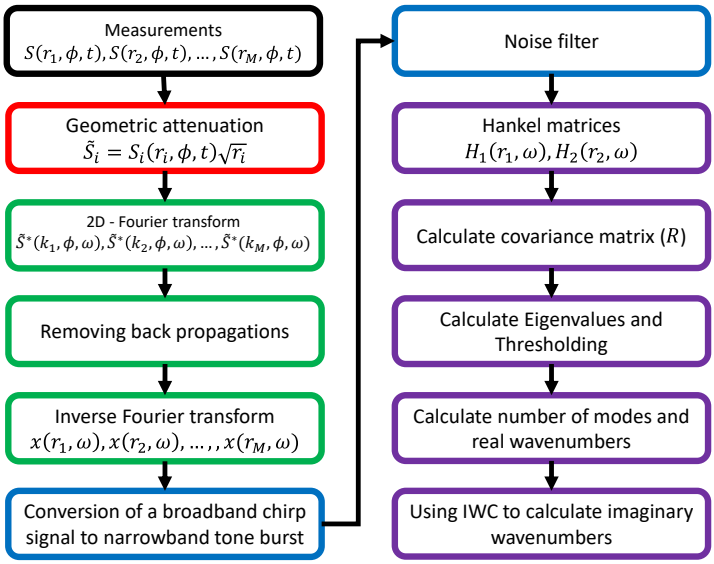

Figure 3: Flowchart of the post processing procedure to estimate complex wavenumbers from virtual or experimentally obtained wavefield data. The flowchart is represented by (colors) based on various steps in the post-processing: In concreto: Correction spreading - Red, Elimination back-propagating waves - Green, Michaels' method for variation in frequency - Blue, and Hybrid TLS-ESPRIT and IWC - Purple

4. Results and discussion

In this section, the material characterization results using the proposed two-stage inversion method for two numerical (virtual experiments) and two experimental case studies (actual measurements) are reported.

First, two numerical simulation studies were conducted, one for a homogeneous C/E plate and another for an orthotropic wooden plate. However,

as finite element simulations assume a controlled and noise-free environment, and in reality environmental fluctuations introduce noise to the experimental measurements, 3% random noise is added to both the real and imaginary wavenumbers deduced from the wavefields calculated in the numerical case studies in order to mimic real life measurement conditions. As such noise levels cause significant errors in the extracted imaginary wavenumbers, especially for higher order Lamb wave modes, only the three fundamental wave modes (A_0, S_0 and SH_0) will be used to identify the set of viscous parameters. Additionally, to avoid supplementary negative effects of higher mode mismatches on the attenuation characteristics, the considered frequency range for the imaginary wavenumber analysis will be limited. Conversely, as the characterization of the elastic parameters is more noise-resistant, the real wavenumbers of all the wave modes are considered in the inversions.

After the numerical validation of the proposed two-stage inversion method, the method is further demonstrated based on input data from experimental wavefield datasets for the characterization of the viscoelastic parameters of a $[45/0/-45/90]_s$ C/E layered laminate and a $[45/-45/0/90]_{3s}$ G/F woven laminate.

4.1. Numerical case study 1: Homogeneous C/E plate

The first case study considers a homogenized viscoelastic orthotropic UD carbon epoxy material with a thickness of 5 mm and a density of 1560 kg/m^3. Details on the complex stiffness tensor can be found in Neau [54], and are listed in column 1 and 2 of Table 1. Lamb wave propagation data was numerically simulated in the frequency range of 15-300 kHz, and analyzed using the hybrid TLS-ESPRIT and IWC method to provide the wavenumber spectrum

on a 15 kHz frequency grid. The results of the inversion procedure are summarized in Table 1. An average relative error of 1.30% for the elastic tensor is observed after Stage I, further reducing slightly to 1.27% after Stage II. The largest error is found to be around 4% for C'_{12}, while the lowest errors are obtained for the shear parameters (C'_{44}, C'_{55}, and C'_{66}) with less than 0.5% error. Additionally, the median absolute deviations, which are represented between brackets in column 4,5, and 6, are extremely small and close to zero for most of the stiffness parameters, implying a good precision and robustness of the inversion method. For what concerns the viscous parameters, the inversion was performed for a restricted frequency range up to 100 kHz and was based on only the first three fundamental modes. The mean percentage error is considerably higher than for the elastic values, around 4.75%, with, at the same time, a median absolute deviation that increased significantly. The largest relative error is obtained for the C''_{22} and C''_{23} parameters. Nevertheless, on the whole, the proposed two stage inversion method managed to characterize both the elasticity and the viscous stiffness parameters with a satisfactorily high accuracy. A visual representation of the wavenumber-frequency pair agreement after inversion is shown in Fig. 4 on top of the optimized dispersion and attenuation curves.

Table 1: PSO inversion results (in GPa) based on a numerically generated COMSOL dataset for a 5 mm thick UD carbon epoxy plate with orthotropic nature, density 1560 kg/m^3, in the *fd* range of 75-1500 kHz·mm. The statistics (median and median absolute deviation) are performed using the output of 20 individual PSO simulations.

	True		Stage I	Stage II	
ij	C'_{ij}	C''_{ij}	C'_{ij}	C'_{ij}	C''_{ij}
11	86.60	7.50	87.95(±0.04)	87.94(±0.02)	7.66(±0.11)
12	9.00	0.30	8.63(±0.04)	8.65(±0.02)	0.30(±0.06)
13	6.40	0.60	6.49(±0.02)	6.49(±0.01)	0.58(±0.11)
22	13.50	0.60	13.39(±0.01)	13.39(±0.00)	0.66(±0.02)
23	6.80	0.25	6.68(±0.01)	6.68(±0.00)	0.30(±0.02)
33	14.00	0.28	14.14(±0.00)	14.14(±0.00)	0.27(±0.06)
44	2.72	0.10	2.71(±0.00)	2.71(±0.00)	0.10(±0.00)
55	4.06	0.12	4.05(±0.00)	4.05(±0.00)	0.12(±0.00)
66	4.70	0.28	4.68(±0.00)	4.68(±0.00)	0.28(±0.00)

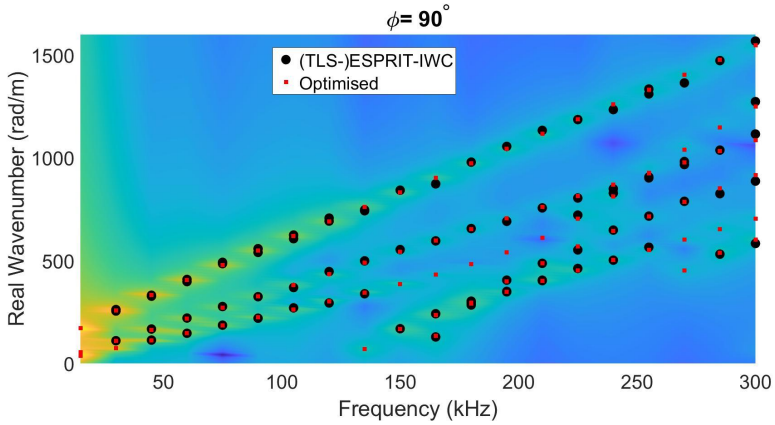

(a)

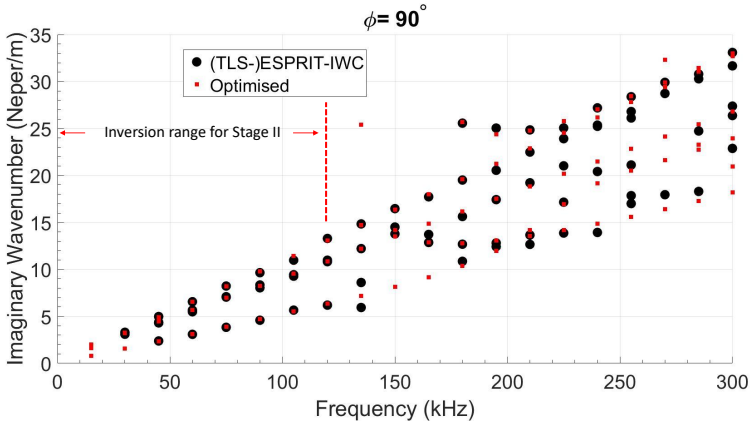

(b)

Figure 4: Wavenumber-frequency pairs calculated via the optimised stiffness values (using SAFE, red dots), compared to the hybrid (TLS)-ESPRIT-IWC wavenumber-frequency pairs (black open circles), extracted from a FEM (2D SAFE in COMSOL) simulation on a 5 mm thick homogeneous C/E plate with orthotropic nature, and overlayed on a) the dispersion curves resulting from the simulated full motion COMSOL data, and b) the attenuation curves results when $\phi = 90$.

4.2. Numerical case study 2: Homogeneous wooden plate

In the second case study, a homogenized orthotropic wooden plate (beech wood) with a thickness of 5 mm and a density of 674 kg/m^3 is considered. Details on the complex stiffness tensor can be found in Bucur and Rocaboy [55], and are listed in column 1 and 2 of Table 2. The excitation signal was assumed to be identical to case 1. The inverted stiffness tensor components are listed in Table 2. The results show that the elastic tensor is inverted with an average 3.62% and 3.58% error after Stage I and Stage II, respectively. Similar to the first case study, the results only slightly improved thanks to Stage II. The relative error levels for beech wood are comparably higher than in case 1 because the elasticity components of beech wood are in absolute value much smaller than those of the homogenized composite material. Consequently, the wavenumber values are much higher in wooden materials for the same frequency, and the slight errors in the numerical modeling and/or noise effects therefore affect the characterized elasticity parameters in an equivalently higher manner. Still, the error levels are within the acceptable range even with 3% random noise, and the precision is high. Again, the relative error levels the for viscous parameters (obtained by restricting the frequency range to 100 kHz) raise to 7%, which is again comparably higher than in case 1 due to the same reason as for the deviations in the elastic parameters. As for case 2, an overlay of the results on the optimized dispersion and attenuation curves of the beech wooden plate is shared in Fig. 5.

Table 2: PSO inversion results (in GPa) based on a numerically generated COMSOL dataset for a 5 mm thick wooden plate with orthotropic nature, density 674 kg/m^3, in the *fd* range of 75-1500 kHz·mm. The statistics (median and median absolute deviation) are performed using the output of 20 individual PSO simulations.

	True		Stage I	Stage II	
ij	C'_{ij}	C''_{ij}	C'_{ij}	C'_{ij}	C''_{ij}
11	17.33	0.87	18.10(±0.00)	18.10(±0.00)	0.95(±0.01)
12	3.03	0.15	3.18(±0.01)	3.19(±0.00)	0.17(±0.00)
13	1.69	0.08	1.82(±0.00)	1.82(±0.00)	0.09(±0.00)
22	3.26	0.16	3.36(±0.02)	3.35(±0.00)	0.17(±0.00)
23	0.74	0.04	0.78(±0.01)	0.78(±0.00)	0.03(±0.00)
33	1.64	0.08	1.55(±0.00)	1.55(±0.00)	0.06(±0.00)
44	0.62	0.03	0.61(±0.00)	0.61(±0.00)	0.03(±0.00)
55	1.09	0.05	1.09(±0.00)	1.09(±0.00)	0.05(±0.00)
66	1.52	0.08	1.51(±0.00)	1.51(±0.00)	0.08(±0.00)

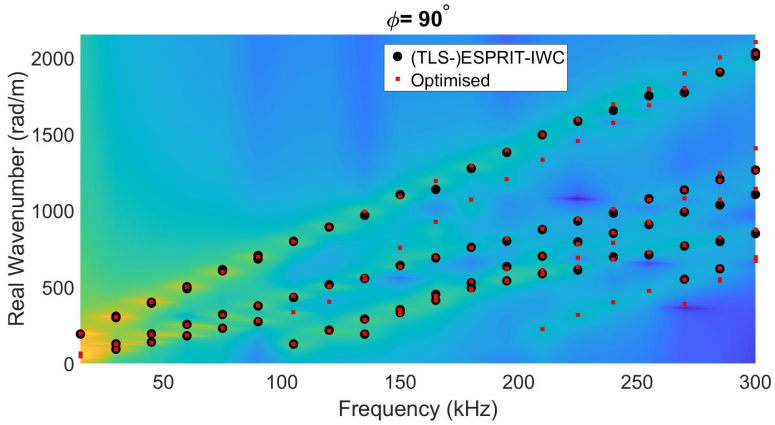

(a)

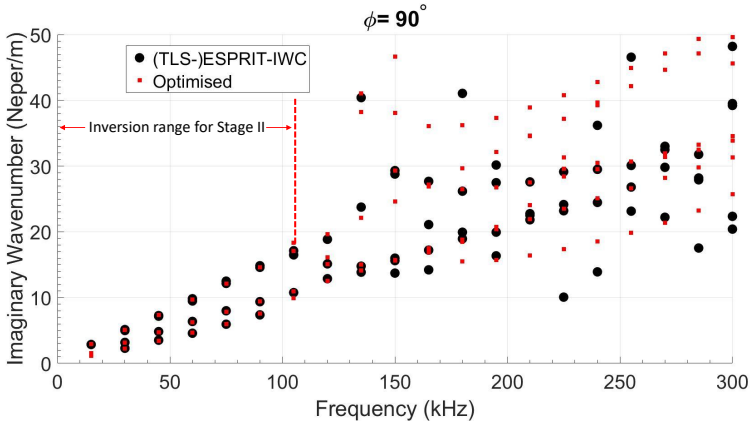

(b)

Figure 5: Wavenumber-frequency pairs calculated via the optimised stiffness values (using SAFE, red dots), compared to the hybrid (TLS)-ESPRIT-IWC wavenumber-frequency pairs (black open circles), extracted from a FEM (2D SAFE in COMSOL) simulation on a 5 mm thick wooden plate with orthotropic nature, and overlayed on a) the dispersion curves resulting from the simulated full motion COMSOL data, and b) the attenuation curves results when when $\phi = 90$.

4.3. Experimental case study 1: Homogenized C/E plate

In the first experimental case study, Lamb wave propagation data has been acquired for a quasi-isotropic $[45/0/-45/90]_s$ C/E laminate with a thickness of 2 mm and a density of 1572 kg/m^3. The individual elasticity properties of the C/E plies are taken from the literature [17], and the homogenized (real) stiffness parameters, listed in column 2 of Table 3, are estimated by accounting for the assumed layer thickness and stacking orientation parameters [56]. Unfortunately, both literature and actual viscous stiffness parameters are unknown for this specimen, and therefore, appropriate target values cannot be shared in this study. At the start of the inversion process, values of 2% of the inverted stiffness parameters are consistently taken as initial guess for viscous stiffness inversion. The inversion process is however restarted with new estimates when the optimization process has converged to the range boundaries to prevent the algorithm to converge to wrong stiffness parameters.

The inverted real and imaginary stiffness parameters are presented in Table 3. For a quasi-isotropic stacking sequence, the elastic tensile parameters in the in-plane directions are expected to be similar ($C'_{11} \approx C'_{22}$), while both should be larger than the value in the out-of-plane direction ($C'_{11} \approx C'_{22} >> C'_{33}$). Similarly, the shear values along the $1-3$ and $2-3$ planes are expected to be similar to each other ($C'_{44} \approx C'_{55}$), and smaller than the shear value in 1-2 direction ($C'_{44} \approx C'_{55} << C'_{66}$). These expected relations are clearly retrieved in the inverted elastic parameters, although the inverted C'_{22} value seems to be notably higher than C'_{11}. Most probably, deviations from an ideal quasi-isotropic stacking may be the cause of the ob-

served difference between the direction 1 and 2. Further, the median absolute deviations, in range of 5%-7%, are much higher compared to numerical case studies because of experimental noise. Still, this is quite satisfactory as in literature, deviations up to 10% are reported to be acceptable for NDT [21]. Similar to numerical cases, only a small frequency range (up to 100 kHz) has been used for the inversion of viscous stiffness parameters. The final viscous stiffness parameters results vary between 1% and 6% of the elastic stiffness parameters, which is similar to literature [17]. The imaginary stiffness parameters in the principal directions (C''_{11}, C''_{22}, and C''_{33}) are typically 3%, whereas the shear viscosity parameters (C''_{44}, C''_{55}, and C''_{66}) are around 2%. The largest deviation was found for the C''_{12} value, i.e. 6% of real stiffness values, and the main reason behind this deviation is possibly the effect of homogenization.

To visualize the accuracy of the inversion results, the dispersion and attenuation curves based on the inverted stiffness parameters are plotted in Fig. 6 as an overlay for the wavenumber-frequency pairs (optimized and determined from the hybrid TLS-ESPRIT&IWC method). As can be seen from the figure, both the real and imaginary inverted wavenumbers match well with the experimentally extracted wavenumber values, and their frequency dependence nicely follows the experimentally obtained dispersion curves shown in the background of Fig. 6(a).

Table 3: PSO inversion results (in GPa) based on a 3D infrared SLDV measurement dataset for a 2 mm thick C/E laminate with orthotropic nature, density 1572 kg/m^3, in the *fd* range of 10-600 kHz·mm. The statistics (median and median absolute deviation) are performed using the output of 20 individual PSO simulations.

	Literature[17]	Stage I	Stage II	
ij	C'_{ij}	C'_{ij}	C'_{ij}	C''_{ij}
11	57.70	47.06(±0.03)	47.06(±0.02)	1.60(±0.00)
12	18.40	19.04(±0.06)	18.99(±0.00)	1.21(±0.00)
13	6.70	3.39(±0.04)	3.43(±0.00)	0.03(±0.00)
22	57.70	60.96(±0.01)	60.96(±0.00)	2.07(±0.01)
23	6.69	10.94(±0.00)	10.94(±0.00)	0.11(±0.00)
33	13.73	9.85(±0.00)	9.85(±0.00)	0.31(±0.00)
44	4.22	2.83(±0.00)	2.83(±0.00)	0.05(±0.00)
55	4.22	2.80(±0.00)	2.80(±0.00)	0.06(±0.00)
66	16.65	17.06(±0.00)	17.06(±0.00)	0.28(±0.00)

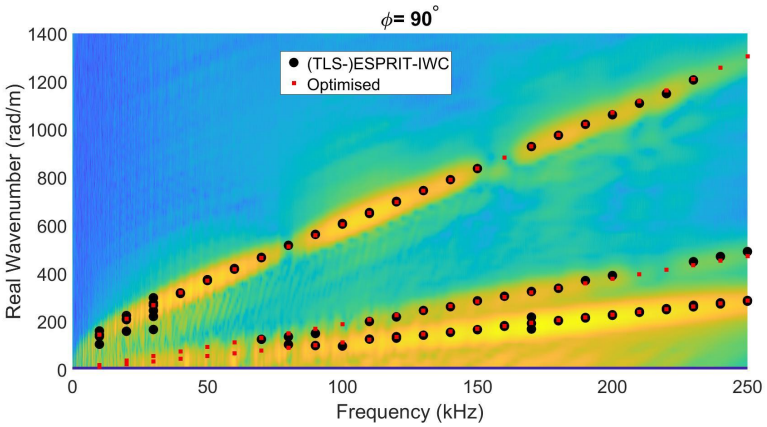

(a)

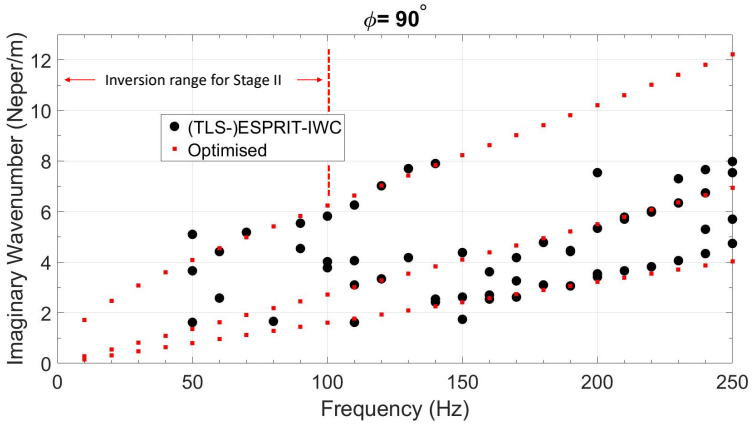

(b)

Figure 6: Wavenumber-frequency pairs calculated via the optimised (homogenized) stiffness values (using SAFE, red dots), compared to the hybrid (TLS)-ESPRIT-IWC wavenumber-frequency pairs (black open circles), extracted from an experiment on a 2 mm thick quasi isotropic C/E plate, and overlayed on a) the dispersion curves resulting from the experimentally obtained full motion data, and b) the attenuation curves results when $\phi = 90$.

4.4. Experimental case study 2: Homogenized G/F woven plate

The second experimental case study considers a $[45/-45/0/90]_{3s}$ G/F woven laminate with a thickness of 6 mm and a density of 1730 kg/m^3. The layer elasticity properties of the glass fiber reinforced polyamide 6 is taken from the literature [57], and the homogenized (real) stiffness parameters are again estimated by using the proper layer thickness and stacking orientation parameters [56]. The latter values, which are used to initialize different parameter sets for the Stage I inversion, are listed in column 2 of Table 4. As in the previous case study, the viscous stiffness parameters were unknown for this specimen. Therefore, the viscous parameters are initially assumed to be 2% of the inverted stiffness parameters, and the inversion process is restarted with new estimates if intermediate optimization results converge near the boundaries of the search domain.

The inverted complex valued stiffness parameters resulting from Stage I and II can be seen in Table 4. As for the experimental case study 2, the deviations are again acceptable. Yet, in this experiment, the median absolute deviation values dropped significantly because of the presence of higher-order Lamb modes in the frequency range 5-300 kHz, leading to a more robust and stable identification of the elastic parameters. For the inversion of the viscous stiffness parameters, using only a small frequency range (up to 100 kHz) the result shows values between 1% and 4% of elastic stiffness parameters. The viscous stiffness parameters for in-plane principal directions (C''_{11} and C''_{22}) are typically 3%, whereas out-of-plane stiffness parameter (C''_{33}) is around 1%. The relative shear viscosity parameters (C''_{44}, C''_{55}, and C''_{66}) are around 2%, similar to experimental case study 1, whereas the other shear

viscosity parameter values (C''_{12}, C''_{13} and C''_{23}) are close to 4% of real stiffness values. In literature, similar attenuation ratios relative to the corresponding elastic parameters have been reported for glass fiber laminate [12], which substantiates the obtained results.

Again, the dispersion and attenuation curves are shared for the optimized stiffness parameters in Fig. 7. The figure shows that the optimized wavenumbers provide a good correspondence with the wavenumbers derived from the experimental measurements, and an excellent match with the experimentally obtained dispersion curves.

Table 4: PSO inversion results (in GPa) based on a 3D infrared SLDV measurement dataset for a 6 mm thick G/F woven laminate with orthotropic nature, density 1730 kg/m^3, in the *fd* range of 30-1800 kHz·mm. The statistics (median and median absolute deviation) are performed using the output of 20 individual PSO simulations.

	Literature[57]	Stage I	Stage II	
ij	C'_{ij}	C'_{ij}	C'_{ij}	C''_{ij}
11	21.43	22.73(±0.00)	22.73(±0.00)	0.69(±0.12)
12	8.51	9.22(±0.00)	9.22(±0.00)	0.41(±0.00)
13	5.41	5.71(±0.00)	5.71(±0.00)	0.23(±0.00)
22	21.43	23.25(±0.01)	23.25(±0.00)	0.78(±0.06)
23	5.41	5.87(±0.01)	5.87(±0.00)	0.24(±0.05)
33	12.3	13.34(±0.00)	13.34(±0.00)	0.10(±0.00)
44	3.28	3.23(±0.00)	3.23(±0.00)	0.07(±0.00)
55	3.28	3.32(±0.00)	3.32(±0.00)	0.09(±0.00)
66	6.46	7.37(±0.00)	7.37(±0.00)	0.15(±0.00)

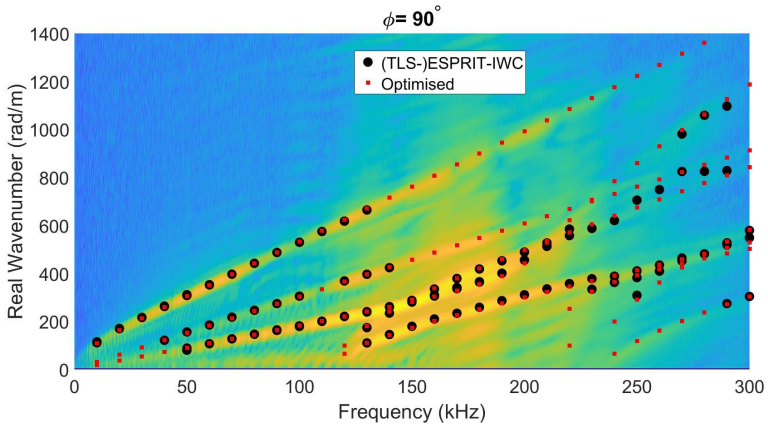

(a)

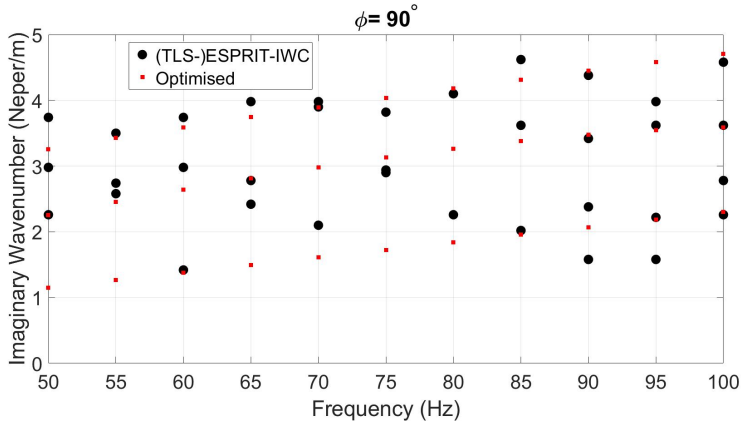

(b)

Figure 7: Wavenumber-frequency pairs calculated via the optimised (homogenized) stiffness values (using SAFE, red dots), compared to the hybrid (TLS)-ESPRIT-IWC wavenumber-frequency pairs (black open circles), extracted from an experiment on a 6 mm thick quasi isotropic G/F woven plate, and overlayed on a) the dispersion curves resulting from the experimentally obtained full motion data, and b) the attenuation curves results when $\phi = 90$.

5. Conclusions

In the present study, a two-stage inversion scheme has been proposed to inversely characterize the complex valued stiffness properties of an arbitrary orthotropic viscoelastic plate from the 3D surface velocity response to a broadband vibrational excitation. The method first converts the 3D wavefield data measured (or simulated) on a star-like configuration into the frequency-wavenumber domain by means of Fast Fourier transform, followed by the extraction of the complex-valued wavenumber values as function of frequency using a hybrid TLS-ESPRIT and IWC method. Then, particle swarm optimization is used to minimize the difference between the experimentally obtained wavenumber values and the computed wavenumber values (and their dispersion) using a fast semi-analytical finite element method as forward model in the optimization. To increase the accuracy, robustness and speed of the inversion process, a two-stage inversion algorithm is adapted. In stage I, the optimization algorithm first identifies 9 elastic parameters, followed by the full characterization of all 18 viscoelastic properties in stage II. The proposed inversion method is validated on a series of synthetic datasets, representative for composite and wooden plates, showing high performance with an average relative error of 2% and 5% on the elastic and viscous parameters, respectively, and small median absolute deviations. Finally, the inversion procedure is applied on experimental data, obtained by 3D Infrared Scanning Laser Doppler Vibrometry, in view of inferring the orthotropic viscoelastic parameters of (woven) composite plates and wood in practice. Thanks to proposed two-stage inversion scheme, elastic and viscous parameters of orthotropic plates can be identified with less computational time and

high accuracy.

Acknowledgements

The authors gratefully acknowledge the financial support from the Fund for Scientific Research-Flanders (FWO Vlaanderen, grants G066618N, G0B9515N, 1S45216N and 12T5418N), and the NVIDIA corporation.

Fonds Wetenschappelijk Onderzoek

References

[1] W. Staszewski, C. Boller, G. R. Tomlinson, Health monitoring of aerospace structures: smart sensor technologies and signal processing, John Wiley & Sons, 2004.

[2] J. Segers, S. Hedayatrasa, G. Poelman, W. Van Paepegem, M. Kersemans, Robust and baseline-free full-field defect detection in complex composite parts through weighted broadband energy mapping of mode-removed guided waves, Mechanical Systems and Signal Processing 151 (2021) 107360.

[3] J. H. Tam, Z. C. Ong, Z. Ismail, B. C. Ang, S. Y. Khoo, Identification of material properties of composite materials using nondestructive vibrational evaluation approaches: A review, Mechanics of Advanced Materials and Structures 24 (12) (2017) 971–986.

[4] K. Sepahvand, S. Marburg, Non-sampling inverse stochastic numerical–experimental identification of random elastic material parameters in composite plates, Mechanical Systems and Signal Processing 54-55

(2015) 172–181. doi:https://doi.org/10.1016/j.ymssp.2014.09.011.
URL https://www.sciencedirect.com/science/article/pii/S0888327014003537

[5] L. F. dos Santos Souza, D. Vandepitte, V. Tita, R. de Medeiros, Dynamic response of laminated composites using design of experiments: An experimental and numerical study, Mechanical Systems and Signal Processing 115 (2019) 82–101. doi:https://doi.org/10.1016/j.ymssp.2018.05.022.
URL https://www.sciencedirect.com/science/article/pii/S0888327018302759

[6] J. H. Tam, Z. C. Ong, C. L. Lau, Z. Ismail, B. C. Ang, S. Y. Khoo, Identification of material properties of composite plates using fourier-generated frequency response functions, Mechanics of Advanced Materials and Structures 26 (2) (2019) 119–128.

[7] D. T. Korontzis, L. Vellios, V. Kostopoulos, On the viscoelastic response of composite laminates, Mechanics of time-dependent materials 4 (4) (2000) 381–405.

[8] J. D. D. Melo, D. W. Radford, Viscoelastic characterization of transversely isotropic composite laminae, Journal of composite materials 37 (2) (2003) 129–145.

[9] M. Matter, T. Gmür, J. Cugnoni, A. Schorderet, Numerical-experimental identification of the elastic and damping properties

in composite plates, Composite Structures 90 (2) (2009) 180–187. doi:https://doi.org/10.1016/j.compstruct.2009.03.001.
URL https://www.sciencedirect.com/science/article/pii/S0263822309000671

[10] M. Schwaar, T. Gmür, J. Frieden, Modal numerical–experimental identification method for characterising the elastic and damping properties in sandwich structures with a relatively stiff core, Composite Structures 94 (7) (2012) 2227–2236. doi:https://doi.org/10.1016/j.compstruct.2012.02.017.
URL https://www.sciencedirect.com/science/article/pii/S0263822312000700

[11] R. Longo, D. Laux, S. Pagano, T. Delaunay, E. Le Clézio, O. Arnould, Elastic characterization of wood by resonant ultrasound spectroscopy (rus): a comprehensive study, Wood science and technology 52 (2) (2018) 383–402.

[12] B. Hosten, M. Deschamps, B. R. Tittmann, Inhomogeneous wave generation and propagation in lossy anisotropic solids. application to the characterization of viscoelastic composite materials, The Journal of the Acoustical Society of America 82 (5) (1987) 1763–1770. arXiv:https://doi.org/10.1121/1.395170, doi:10.1121/1.395170.
URL https://doi.org/10.1121/1.395170

[13] S. Dahmen, H. Ketata, M. H. B. Ghozlen, B. Hosten, Elastic constants measurement of anisotropic olivier wood plates using air-coupled trans-

ducers generated lamb wave and ultrasonic bulk wave, Ultrasonics 50 (4-5) (2010) 502–507.

[14] A. Castellano, P. Foti, A. Fraddosio, S. Marzano, M. D. Piccioni, Mechanical characterization of cfrp composites by ultrasonic immersion tests: Experimental and numerical approaches, Composites Part B: Engineering 66 (2014) 299–310. doi:https://doi.org/10.1016/j.compositesb.2014.04.024.
URL https://www.sciencedirect.com/science/article/pii/S1359836814001802

[15] D. Barazanchy, W. Roth, V. Giurgiutiu, A non-destructive material characterization framework for retrieving a stiffness matrix using bulk waves, Composite Structures 185 (2018) 27–37.

[16] A. Martens, M. Kersemans, J. Daemen, E. Verboven, W. Van Paepegem, J. Degrieck, S. Delrue, K. Van Den Abeele, Numerical study of the time-of-flight pulsed ultrasonic polar scan for the determination of the full elasticity tensor of orthotropic plates, Composite Structures 180 (2017) 29–40.

[17] A. Martens, M. Kersemans, J. Daemen, E. Verboven, W. Van Paepegem, S. Delrue, K. Van Den Abeele, Characterization of the orthotropic viscoelastic tensor of composites using the ultrasonic polar scan, Composite Structures 230 (2019) 111499. doi:https://doi.org/10.1016/j.compstruct.2019.111499.
URL https://www.sciencedirect.com/science/article/pii/S0263822319311274

[18] M. Sale, P. Rizzo, A. Marzani, Semi-analytical formulation for the guided waves-based reconstruction of elastic moduli, Mechanical Systems and Signal Processing 25 (6) (2011) 2241–2256.

[19] A. Marzani, L. De Marchi, Characterization of the elastic moduli in composite plates via dispersive guided waves data and genetic algorithms, Journal of intelligent material systems and structures 24 (17) (2013) 2135–2147.

[20] V. Takahashi, M. Lematre, J. Fortineau, M. Lethiecq, Elastic parameters characterization of multilayered structures by air-coupled ultrasonic transmission and genetic algorithm, Ultrasonics 119 (2022) 106619.

[21] P. Kudela, M. Radzienski, P. Fiborek, T. Wandowski, Elastic constants identification of fibre-reinforced composites by using guided wave dispersion curves and genetic algorithm for improved simulations, Composite Structures 272 (2021) 114178.

[22] L. Araque, L. Wang, A. Mal, C. Schaal, Advanced fuzzy arithmetic for material characterization of composites using guided ultrasonic waves, Mechanical Systems and Signal Processing 171 (2022) 108856. doi:https://doi.org/10.1016/j.ymssp.2022.108856.
URL https://www.sciencedirect.com/science/article/pii/S088832702200053X

[23] W.-J. Yan, D. Chronopoulos, S. Cantero-Chinchilla, K.-V. Yuen, C. Papadimitriou, A fast bayesian inference scheme for identification of local structural properties of layered composites based on wave

and finite element-assisted metamodeling strategy and ultrasound measurements, Mechanical Systems and Signal Processing 143 (2020) 106802. doi:https://doi.org/10.1016/j.ymssp.2020.106802.
URL https://www.sciencedirect.com/science/article/pii/S0888327020301886

[24] F. Marchetti, N. Roozen, J. Segers, K. Ege, M. Kersemans, Q. Leclère, Experimental methodology to assess the dynamic equivalent stiffness properties of elliptical orthotropic plates, Journal of Sound and Vibration 495 (2021) 115897. doi:https://doi.org/10.1016/j.jsv.2020.115897.
URL https://www.sciencedirect.com/science/article/pii/S0022460X20307367

[25] F. Marchetti, K. Ege, Q. Leclère, N. Roozen, On the structural dynamics of laminated composite plates and sandwich structures; a new perspective on damping identification, Journal of Sound and Vibration 474 (2020) 115256. doi:https://doi.org/10.1016/j.jsv.2020.115256.
URL https://www.sciencedirect.com/science/article/pii/S0022460X20300870

[26] B. Hosten, Stiffness matrix invariants to validate the characterization of composite materials with ultrasonic methods, Ultrasonics 30 (6) (1992) 365–370. doi:https://doi.org/10.1016/0041-624X(92)90092-Z.
URL https://www.sciencedirect.com/science/article/pii/0041624X9290092Z

[27] H. Fathi, S. Kazemirad, V. Nasir, A nondestructive guided wave propa-

gation method for the characterization of moisture-dependent viscoelastic properties of wood materials, Materials and Structures 53 (6) (2020) 1–14.

[28] W. Ostachowicz, P. Kudela, M. Krawczuk, A. Zak, Guided waves in structures for SHM: the time-domain spectral element method, John Wiley & Sons, 2011.

[29] P. S. V. H. Manual, Operating instructions of polytec scanning vibrometer psv-500-3d, https://www.polytec.com/int/vibrometry/products/full-field-vibrometers/psv-500-3d-scanning-vibrometer (accessed 17-August-2022).

[30] A. Gallina, L. Ambrozinski, P. Packo, L. Pieczonka, T. Uhl, W. J. Staszewski, Bayesian parameter identification of orthotropic composite materials using lamb waves dispersion curves measurement, Journal of Vibration and Control 23 (16) (2017) 2656–2671.

[31] A. H. Orta, S. Azadi, S. Hedayatrasa, N. B. Roozen, W. Van Paepegem, M. Kersemans, K. Van Den Abeele, Identification of the orthotropic elastic tensor of composites using full field lamb wave energy velocities and dispersion curves, in: Quantitative Nondestructive Evaluation, Vol. 85529, American Society of Mechanical Engineers, 2021, p. V001T06A006.

[32] D. Alleyne, P. Cawley, A two-dimensional fourier transform method for the measurement of propagating multimode signals, The Journal of the Acoustical Society of America 89 (3) (1991) 1159–1168.

[33] L. Zeng, L. Huang, X. Cao, F. Gao, Determination of lamb wave phase velocity dispersion using time–frequency analysis, Smart Materials and Structures 28 (11) (2019) 115029.

[34] L. Draudviliene, O. Tumsys, L. Mazeika, E. Zukauskas, Estimation of the lamb wave phase velocity dispersion curves using only two adjacent signals, Composite Structures 258 (2021) 113174. doi:https://doi.org/10.1016/j.compstruct.2020.113174.
URL https://www.sciencedirect.com/science/article/pii/S0263822320331007

[35] X. Cao, L. Zeng, J. Lin, Lamb wave mode decomposition and reconstruction based on the viscoelastic propagation model, Structural Health Monitoring 20 (1) (2021) 25–45.

[36] J. B. Harley, J. M. Moura, Sparse recovery of the multimodal and dispersive characteristics of lamb waves, The Journal of the Acoustical Society of America 133 (5) (2013) 2732–2745.

[37] A. Geslain, S. Raetz, M. Hiraiwa, M. Abi Ghanem, S. Wallen, A. Khanolkar, N. Boechler, J. Laurent, C. Prada, A. Duclos, et al., Spatial laplace transform for complex wavenumber recovery and its application to the analysis of attenuation in acoustic systems, Journal of Applied Physics 120 (13) (2016) 135107.

[38] J. Berthaut, M. Ichchou, L. Jezequel, K-space identification of apparent structural behaviour, Journal of Sound Vibration 280 (3-5) (2005) 1125–1131.

[39] Q. Chen, K. Xu, D. Ta, High-resolution lamb waves dispersion curves estimation and elastic property inversion, Ultrasonics 115 (2021) 106427.

[40] M. Mazzotti, C. Sugino, E. Kohtanen, A. Erturk, M. Ruzzene, Experimental identification of high order lamb waves and estimation of the mechanical properties of a dry human skull, Ultrasonics 113 (2021) 106343.

[41] A. H. Orta, M. Kersemans, K. Van Den Abeele, On the identification of orthotropic elastic stiffness using 3d guided wavefield data, Sensors 22 (14) (2022) 5314.

[42] I. Bartoli, A. Marzani, F. L. di Scalea, E. Viola, Modeling wave propagation in damped waveguides of arbitrary cross-section, Journal of Sound and Vibration 295 (3-5) (2006) 685–707.

[43] A. H. Orta, M. Kersemans, K. Van Den Abeele, The dispersion box, https://github.com/adilorta/The-Dispersion-Box.git (2022 (accessed 12-January-2022)).

[44] A. H. Orta, M. Kersemans, K. Van Den Abeele, A comparative study for calculating dispersion curves in viscoelastic multi-layered plates, Composite Structures 294 (2022) 115779. doi:https://doi.org/10.1016/j.compstruct.2022.115779.
URL https://www.sciencedirect.com/science/article/pii/S0263822322005530

[45] R. Cui, F. Lanza di Scalea, On the identification of the elastic properties of composites by ultrasonic guided waves and optimization algorithm, Composite Structures 223 (2019) 110969.

doi:https://doi.org/10.1016/j.compstruct.2019.110969.
URL https://www.sciencedirect.com/science/article/pii/S0263822319307147

[46] A. H. Orta, J. Segers, J. Vandendriessche, N. Roozen, W. V. Paepegem, M. Kersemans, K. V. D. Abeele, Characterization of the orthotropic elastic tensor of composites using full-field Lamb waves, in: Forum Acusticum, Lyon, France, 2020, pp. 3319–3326. doi:10.48465/fa.2020.0909.
URL https://hal.archives-ouvertes.fr/hal-03235483

[47] Y. Shi, et al., Particle swarm optimization: developments, applications and resources, in: Proceedings of the 2001 congress on evolutionary computation (IEEE Cat. No. 01TH8546), Vol. 1, IEEE, 2001, pp. 81–86.

[48] C. A. Leckey, K. R. Wheeler, V. N. Hafiychuk, H. Hafiychuk, D. A. Timuçin, Simulation of guided-wave ultrasound propagation in composite laminates: Benchmark comparisons of numerical codes and experiment, Ultrasonics 84 (2018) 187–200. doi:https://doi.org/10.1016/j.ultras.2017.11.002.
URL https://www.sciencedirect.com/science/article/pii/S0041624X17305462

[49] M. V. Predoi, M. Castaings, B. Hosten, C. Bacon, Wave propagation along transversely periodic structures, The Journal of the Acoustical Society of America 121 (4) (2007) 1935–1944.

[50] C. Ramadas, Three-dimensional modeling of lamb wave attenuation due to material and geometry in composite laminates, Journal of Reinforced Plastics and Composites 33 (9) (2014) 824–835.

[51] J. E. Michaels, S. J. Lee, A. J. Croxford, P. D. Wilcox, Chirp excitation of ultrasonic guided waves, Ultrasonics 53 (1) (2013) 265–270.

[52] Y. Hua, T. K. Sarkar, On svd for estimating generalized eigenvalues of singular matrix pencil in noise, in: 1991., IEEE International Sympoisum on Circuits and Systems, IEEE, 1991, pp. 2780–2783.

[53] W. Y. Yang, MATLAB/Simulink for Digital Signal Processing, Won Y. Yang, 2015.

[54] G. Neau, Lamb waves in anisotropic viscoelastic plates. study of the wave fronts and attenuation, Ph.D. thesis, L'Universite de Bordeaux (2003).

[55] V. Bucur, F. Rocaboy, Surface wave propagation in wood: prospective method for the determination of wood off-diagonal terms of stiffness matrix, Ultrasonics 26 (6) (1988) 344–347. doi:https://doi.org/10.1016/0041-624X(88)90033-9.
URL https://www.sciencedirect.com/science/article/pii/0041624X88900339

[56] J. N. Reddy, Mechanics of laminated composite plates and shells: theory and analysis, CRC press, 2003.

[57] D. P. Raghavalu Thirumalai, T. Løgstrup Andersen, A. Lystrup, Influence of moisture absorption on properties of fiber reinforced polyamide

6 composites, in: Proceedings of the 26th Annual Technical Conference of the American Society for Composites 2011 and the 2nd Joint US-Canada Conference on Composites, DEStech Publications, Inc., 2011, pp. 500–510.